Energy distributing and thermodynamic characteristics of a coupling near-isothermal compressed air energy storage system

Ruixiong Li[a], Rui Tao[a], Xiaojun Feng[b], Erren Yao[a,*], Haoran Zhang[c,*], Lanning Ling[a], Huanran Wang[a]

[a] *School of Energy and Power Engineering, Xi'an Jiaotong University, Xi'an 710049, Shaanxi, China*

[b] *Xi'an Modern Chemistry Research Institute, Xi'an 710065, Shaanxi, China*

[c] *The Bartlett School of Sustainable Construction, University College London, London, United Kingdom*

[*] Corresponding author

E-mail addresses: erren@xjtu.edu.cn (E. Yao)

Abstract

Intermittent renewable energy generation systems bring serious adverse impacts to the stable operation of the grid. In this regard, large-scale compressed air energy storage (CAES) systems with the potential to serve as long-term could be a solution for their optimal utilization. However, in a conventional CAES, most of the electricity is transformed into heat which passed into heat exchange mediums leads to serious heat transfer losses. In this study, a novel CAES system employing a Kalina cycle to effectively utilize the pre-compression heat in a near-isothermal compressed air process, is proposed and its holistic dynamic model is developed and presented for a deeper understanding of performance. The results showed that a near-isothermal compression undertakes the responsibilities of storing pressure potential energy, and the adiabatic pre-compression process helping in raising the inlet pressure of the liquid piston is primarily for storing thermal energy. In addition, the Kalina cycle working in the adiabatic pre-compression process achieves a 2.7% improvement in the electrical efficiency. The thermal energy storage temperature was highlighted as the key factor in the energy allocation among the Kalina cycle, the thermal energy storage component, and the energy releasing sub-system in the proposed system. Through a systematic analysis of the proposed system performance, the highest electrical efficiency attained was 65.1% with a 353 K storage temperature.

Keywords: Compressed air energy storage, Adiabatic compression, Near-isothermal compression, Thermodynamic evaluation

1.Introduction

Isothermal compressed air energy storage (ICAES) is an evolving technology that relies on the near-isothermal compression to achieve energy storage potential in addition to the near-isothermal expansion processes to release the stored energy. This technology eliminates the need for a heat source prior to the expansion process and is demonstrated to provide the highest round-trip efficiency (RTE) compared to conventional compressed air energy storage (CAES) systems, including adiabatic compressed air energy storage (ACAES) and diabatic compressed air energy storage (DCAES), which release energy by adiabatically expanding air by using an air-expander [1]. In such systems, the compressing or expanding process are either isothermal or adiabatic depending on the thermal conductivity of the system limit and the rate at which the process occurs. A very fast process where little heat is transferred between the system and its surroundings generally depicted

as an adiabatic process, while a slow process where the system temperature remains constant is considered isothermal [2]. Therefore, to achieve a near-isothermal process in ICAES applications, a large surface area is required to improve the heat transfer during compression or expansion. This was investigated thoroughly in the literature, considering two research directions.

The first line of research is investigating the use of a liquid piston to achieve isothermal compressed air. Thibault et al. discussed the internal airflow characteristics during slow piston compression inside a compression chamber with a very low stroke-to-bore ratio [3]. In another study, Vikram et al. compared liquid piston-based ICAES systems used to store air in an underwater container, and confirmed that the round-trip efficiency can be significantly improved to reach 62% by designing compressors and expanders operating under near-isothermal conditions [4]. It has been demonstrated in the literature that liquid piston compressors are extremely efficient at achieving near-isothermal compression. However, the compression efficiency of the liquid piston can be further improved through the use of heat transfer enhancement mechanism inside the compression chamber.

Moreover, Jacob et al. studied experimentally the effect of porous media in a high pressure (7–210 bar) liquid piston air compressors and expanders. They reported that the efficiency was increased by 13% in the compression process and 23% in the expansion process, while the porous media were uniformly distributed [5]. Perry et al. proposed a novel liquid piston with a gas–solid–liquid three-layer heat transfer structure. In their study, a porous medium was used to enhance the heat transfer between air and liquid, resulting in an 11% compression efficiency increase at a compression ratio of 7 [5, 6]. In another study, Vikram et al. experimentally tested a novel heat transfer enhancement technique using a metal wire mesh in a liquid piston compressor. They found that the metal wire mesh improved the compression isothermal efficiency to 88–90% compared to the base case efficiency of 82–84% [7].

The second line of research was mainly concentrated on cooling the compressed air using water sprays, which can enhance heat transfer and maintain the air at nearly-constant temperatures. In this case, injecting a small amount of atomized water droplets can provide a large surface area. Moreover, water has a large heat capacity, aiding in mitigating the air temperature change [7]. Water injection has been demonstrated in a conventional solid piston for CAES [8], and is commonly used in industrial gas turbines and aero engines for the purpose of heat transfer enhancement [9]. Besides,

in the last few years, this method has been employed in liquid piston compressor applications. Jeffrey et al. examined balancing the intermittency of renewable energy resources through employing an offshore CAES system that combines near-isothermal compression and expansion processes via water spray injection with air storage in saline aquifers. The results showed that the proposed 200 MW system could achieve an round-trip efficiency of 77% [10]. In another work, Ghady et al. compared comprehensively the physical parameters of a mechanical piston with water injection and a liquid piston with an integrated heat exchanger. They concluded that the liquid piston with an integrated heat exchanger provides strong isothermal compression and expansion with a minimal air-water temperature gradient [11].

Generally, the liquid piston compressed air technique became widely accepted in ICAES applications due to its easy operation and simple structure [11]. However, the pumps in a liquid piston system operate inefficiently due to the drastic change in pump back pressure in the charge stage. To improve the thermal performance of the liquid piston, an efficient method of adiabatically pre-compressing air before it enters the liquid piston was proposed [12]. This can certainly improve the pump's efficiency. However, the compression heat with a high temperature source from the adiabatically compressed air needs to be stored in a thermal energy storage (TES) accumulator in the charge stage. This causes some exergy loss along with extra investment costs compared a with conventional ICAES. Considering for this, it is necessary for utilizing the compressing heat sourced with high temperature from adiabatic compression process in order to improve the energy utilization. Here, a Kalina cycle characterized with lower exergy destruction rate is employed to convert the pre-compressing heat into electricity in charge stage; this cycle appears as the most promising alternatives for producing electricity from low- and medium-grade waste heat resources.

The main feature of the Kalina cycle is the use of a water-ammonia mixture, which provides major benefits compared to using a pure working fluid. This is because the saturation temperature of the ammonia-water mixture in a two-phase region is not constant during the heat absorption process at constant pressure [13, 14]. This causes the temperature profile of the ammonia-water mixture to be closer to the temperature of the heat source than in the case of a pure working fluid. As a result, the exergy destruction rate is significantly lower in the Kalina cycle compared to other waste heat recovery cycles. This is due in large part to the lower temperature difference between the working fluid and the heat source [13, 15]. In addition, the turbines of the Kalina cycle are smaller

which remarkably appears as an advantage for it. Therefore, in this study, a Kalina cycle is employed to convert the pre-compressing heat into electricity. Noticeably, the combination of a Kalina cycle and an ACAES has been thoroughly discussed in one of the author's previous study [14]. It was highlighted that the use of Kalina cycles leads to positive results in terms of improving the thermal performance of the ACAES. Nevertheless, a number of researchers also focused on investigating similar combined systems and discussed their superiority compared to the individual conventional systems. In this paper, the proposed system is an upgraded CAES system, which is not only capable of achieving isothermal compressed air but also improves the utilization of adiabatic pre-compression heat. On this basis, the main objective of this study is to provide an accurate and comprehensive evaluation of the proposed system's performance through the building of detailed thermodynamic models. The developed models will then be used to explore the effect of some key system parameters on the thermal performance of the proposed system.

The overall outline of this paper is organized as follows: Section 2 describes the schematic diagram of the proposed system. Then, the developed thermodynamic model of each component is presented in Section 3. Section 4 presents the performance analysis of the system. Finally, the conclusions are summarized in Section 5.

2. System Description

Fig. 1 presents a schematic of the proposed energy system. The system is composed of three subsystems: a compressed air energy storage system, a Kalina cycle unit employing ammonia-water mixtures as a working fluid, and a heat pump cycle utilizing lithium bromide and R245fa to recover waste heat. In the charging stage, ambient air is first compressed by a pre-compressor (streams 1 to 8) and stored in a buffer tank. Then, this part of air is driven as input into the liquid piston to undergo further compression to achieve a set pressure value (streams 12 to 13). Here, the pre-compressor and the liquid piston are both driven by using redundant power during a low power load period. The difference between those two components is that the pre-compressor operates based on an adiabatic process, while the liquid piston compresses air under a near-isothermal condition. A certain amount of compression heat is produced during the pre-compression process, which is used to power a Kalina cycle. The rest of the thermal energy, which is characterized by a temperature below 373.15 K, is stored in a thermal energy storage tank, employing water as the thermal energy storage medium.

Moreover, in the discharging stage, the stored air absorbs the stored thermal energy first within the preheater. Then, the air is heated again by the hot flow medium from the heat pump cycle in a reheater. After this process, the high-temperature, high-pressure air expands in the air expander to generate electricity (streams 15 to 28).

Nevertheless, compared with conventional ACAES applications, the proposed system is characterized by lower compression heat production than the existing near-isothermal compression process. Simultaneously, the outlet temperature of the pre-compressor is relatively lower compared to the case in conventional systems due to the relatively smaller adiabatic compression ratio. Thus, a Kalina cycle is employed to convert the low-grade compression heat into electricity. Moreover, in the discharge stage, a thermally coupled hybrid compression-absorption heat pump (HP) is used in this work to achieve high-temperature output, consisting of a compression sub-cycle and an absorption sub-cycle. More detailed information on the Kalina cycle and the HP cycle employed in this work can be found from Refs. [14] and [16].

3. Mathematical Model

In the following analysis, the mass and energy conservation laws of each component are listed and presented to obtain the corresponding thermodynamic properties. To aid the evaluation and analysis, the mathematical model and the thermodynamic analysis of the proposed system are developed under the following assumptions [1, 12]:

(1) The ambient air temperature and pressure are assumed to be constant at 298.15 K and 101.325 kPa, respectively.

(2) The flow pressure drops in pipes and the local loss in heat exchangers are neglected.

(3) The air composition is considered to be 78.12% nitrogen, 20.96% oxygen, and 0.92% argon.

(4) The thermo-physical properties of the employed materials are constant.

(5) The hot medium in the condenser is cooled by water at atmospheric temperature.

3.1 CAES cycle

(1) Air compressor

A pre-compression process achieves by using low-pressure compressor, which compresses ambient air to a medium pressure. The power consumption for the low-pressure compressor can be calculated as follows:

$$\dot{W}_{\mathrm{COMP}} = \dot{m}_{\mathrm{COMP}} \left(h_{\mathrm{COMP,s}}^{\mathrm{out}} - h_{\mathrm{COMP}}^{\mathrm{in}} \right) \tag{1}$$

where $h_{\mathrm{COMP,s}}^{\mathrm{out}}$ and $h_{\mathrm{COMP}}^{\mathrm{in}}$ are the outlet and inlet entropy of air, respectively. The outlet temperature is given by the product of inlet temperature and compression ratio, as following equation:

$$T_{\mathrm{COMP,s}}^{\mathrm{out}} = T_{\mathrm{COMP}}^{\mathrm{in}} \left(\frac{\pi_{\mathrm{COMP}}^{(n-1)/n} - 1}{\eta_{\mathrm{COMP}}} + 1 \right) \tag{2}$$

where n is the compression polytropic exponent.

$$\eta_{\mathrm{COMP}} = \frac{h_{\mathrm{COMP,s}}^{\mathrm{out}} - h_{\mathrm{COMP}}^{\mathrm{in}}}{h_{\mathrm{COMP}}^{\mathrm{out}} - h_{\mathrm{COMP}}^{\mathrm{in}}} \tag{3}$$

(2) Liquid piston compressor

The liquid piston compressor brings the air pressure from medium to a higher value, and in this process the pressurized-water is pumped into liquid piston cavity. A single compression stroke of a liquid piston is similar to a reciprocating piston compression process, and contains four portions: intake, compression, exhaust and expansion; the specific working process of liquid piston has been discussed in Refs. [11, 17]. By neglecting the mass transfer between gas and liquid, the power consumption can be calculated by:

$$\dot{W}_{\mathrm{PUMP1}} = \dot{m}_w \left(p_w^{\mathrm{in}} - p_w^{\mathrm{out}} \right) / \rho_w \tag{4}$$

where p_w^{in} and p_w^{out} represent the water pressure at the inlet and outlet of pump; associated with the continuity equation for the gas-pressurized process, $\dot{W}_{\mathrm{PUMP1}}$ can then be expressed as:

$$\dot{W}_{\mathrm{PUMP1}} = \left(p_w^{\mathrm{in}} - p_w^{\mathrm{out}} \right) \frac{dV_a}{dt} \tag{5}$$

Here, the compression performance can be characterized of temperature of air inside liquid piston, and according to the law of energy conservation, the non-equilibrium model to study heat transfer between air and water inside liquid piston cavity can be shown as:

$$m_a c_a \frac{dT_a}{dt} = -U_{a,w} A_{a,w} \left(T_a - T_w \right) - U_a A_a \left(T_a - T_{\mathrm{amb}} \right) - p_a \frac{dV_a}{dt} \tag{6}$$

$$m_w c_w \frac{dT_w}{dt} = -U_{a,w} A_{a,w} \left(T_w - T_a \right) - U_w A_w \left(T_w - T_{\mathrm{amb}} \right) + \dot{m}_w c_w \left(T_{\mathrm{amb}} - T_w \right) \tag{7}$$

where Eqs. (6) and (7) are the governing equation of air-side and liquid-side, respectively. the subscript 'a' and 'w' identify the air and water inside the liquid piston, and subscript 'a, w' represents contact surface between gas and liquid. A, c, T, V and p are the contact area, specific heat capacity, temperature, volume and pressure of working medium in the vessel, respectively. U is the heat transfer coefficient, and U_a, U_w can be expressed as follows [18]:

$$U_a A_a = 1 \Big/ \left[\left(\frac{1}{h_{i,a} A_{i,a}} \right) + \left(\frac{t_T}{k_T A_{\text{ave},a}} \right) + \left(\frac{1}{h_O A_{O,a}} \right) \right] \tag{8}$$

$$U_w A_w = 1 \Big/ \left[\left(\frac{1}{h_{i,w} A_{i,w}} \right) + \left(\frac{t_T}{k_T A_{\text{ave},w}} \right) + \left(\frac{1}{h_O A_{O,w}} \right) \right] \tag{9}$$

where $h_{i,a}$ is the inner heat transfer coefficients, and can be evaluated using following equation with regard to the either expansion or compression portion of the liquid piston [12, 19]:

$$Nu_{i,a} = 3.25 Ra_{i,a}^{*0.272} F^{0.765} \tag{10}$$

where $Ra_{i,a}^{*}$ and F stand for the modified Rayleigh number and the shape factor, and are expressed as:

$$F = \frac{V}{A_{i,a} D} \tag{11}$$

$$Ra_{i,a}^{*} = \frac{\rho_a^{\,2} g \alpha_V \left(T_a - T_L\right) H^3 C_v}{\mu \lambda} \tag{12}$$

where V, D and $A_{i,a}$ are the volume, internal diameter and internal surface area of gas phase composition in liquid piston compressor. α_V and T_L represent the thermal expansion coefficient and temperature of air; H, μ and λ denote the air phase height in air-water co-existed tank, dynamic viscosity of air and thermal conductivity of air, respectively.

With regarding to the intake or expansion portion of the liquid piston, $h_{i,a}$ can be calculated using the following equation [7, 20, 21]:

$$Nu_{i,a} = 0.56 Re_d^{0.67} + 0.104 Ra_{i,a}^{0.352} \tag{13}$$

where Re_d is the Reynolds number of air at the inlet of liquid piston, and can be calculated as follows:

$$Re_d = \frac{\rho_a v_a d}{\mu} \tag{14}$$

Rayleigh number $Ra_{i,a}$ is calculated as:

$$Ra_{i,a} = \frac{\rho_a^{\,2} g \alpha_V \left(T_a - T_L\right) H^3 C_p}{\mu \lambda} \tag{15}$$

Finally, the outer heat transfer coefficient h_O is modeled by assuming forced convection over a vertical cylinder under a representative outdoor wind velocity of ~3 m/s based on the Churchill and Bernstein correlation [22].

Moreover, the Nusselt number under different conditions can be used to evaluate the gas-to-liquid

heat transfer coefficient $U_{a,w}$ [18],

$$Nu_{a,w}=\begin{cases}0.54Ra_{a,w}^{1/4},\ (T_w>T_a)\\ 0.52Ra_{a,w}^{1/5},\ (T_w<T_a)\\ 0.54Ra_{a,w}^{1/4}+0.52Ra_{a,w}^{1/5}/2,\ (T_a=T_w)\end{cases} \tag{16}$$

It is known that the Nusselt number reflects the convective heat transfer capacity, and is the ratio of convection heat to conduction heat across the flow boundary layer. Noticeably, under identical temperature conditions ($T_a=T_w$), convective heat transfer still exists due to the continuous changing volume of air, and the temperature difference between the wall and the working medium in liquid piston. In Eq. (16), the Nusselt number correlates in terms of the Rayleigh number $Ra_{a,w}$, which is determined as following,

$$Ra_{a,w}=PrGr=\frac{\upsilon}{\alpha}\frac{g\beta L^3\Delta T}{\upsilon^2} \tag{17}$$

where, Pr and Gr represent Prandtl and Grashof number.

To validate above mentioned models, a 100 kW near-isothermal compression system was constructed in our lab, and consisted of two 20 m^3 air-water co-existed tank and water pump. A detailed description for this system has be published in Ref. [12]. In this study, the variation of air temperature in compression portion in the experiment system is employed for the model validation, shown as Fig. 2. It can be found that the experimental data were accordant to the theoretical prediction, and the maximum error between experimental and theoretical values is 2%.

(3) Air storage tank

According to the law of energy conservation, the relationship between internal energy within the pressured air and energy dissipation of air storage device is established.

$$\frac{d(me)}{dt}=\left(\dot{m}_{\text{in}}h_{\text{in}}-\dot{m}_{\text{out}}h_{\text{out}}\right)-U_{\text{AST},O}A\left(T_{\text{wall},O}-T_{\text{amb}}\right) \tag{18}$$

where the first term in Eq. (18) on the right hand side accounts for energy transfer due to injection/withdraw of air from the cavern, and the second term quantifies the heat transfer between ambient air and cavern's walls. $U_{\text{AST},O}$ is the heat transfer coefficient [23, 24].

(4) Air expander

The power produced by air expander is calculated via the difference between input and output entropy:

$$\dot{W}_{\text{EXP}}=\dot{m}_{\text{EXP}}\left(h_{\text{EXP}}^{\text{in}}-h_{\text{EXP,s}}^{\text{out}}\right) \tag{19}$$

where $h_{\text{EXP,s}}^{\text{out}}$ is the actual enthalpy at the outlet of air expander, and its relationship with isentropic efficiency is depicted:

$$\eta_{\mathrm{EXP}}=\frac{h_{\mathrm{EXP}}^{\mathrm{in}}-h_{\mathrm{EXP}}^{\mathrm{out}}}{h_{\mathrm{EXP}}^{\mathrm{in}}-h_{\mathrm{EXP,s}}^{\mathrm{out}}} \tag{20}$$

Actual outlet temperature of isentropic expanded air from air expander can be expressed as:

$$T_{\mathrm{EXP,s}}^{\mathrm{out}}=T_{\mathrm{EXP}}^{\mathrm{in}}\left[1-\eta_{\mathrm{EXP}}\left(1-\pi_{\mathrm{EXP}}^{(n-1)/n}\right)\right] \tag{21}$$

(5) TES model

For the proposed system, the storage temperature in TES keeps in a lower value, less than 373 K. Thus, in thermal energy storage or release process there is no phase change in water medium.

$$\sum \dot{Q}_{\mathrm{TES}}=\sum \dot{Q}_{\mathrm{TES}} \tag{22}$$

where $\sum \dot{Q}_{\mathrm{TES}}$ and $\sum \dot{Q}_{\mathrm{TES}}$ are the thermal energy stored and released in TES.

(6) Preheater and intercooler

The heat duty of preheater and intercooler is calculated by using a simple energy balance on one of the streams:

$$\dot{Q}_{\mathrm{PH}}=\dot{m}_{\mathrm{PH}}^{\mathrm{hot}}c_p^{\mathrm{hot}}\left(T_{\mathrm{PH}}^{\mathrm{in,hot}}-T_{\mathrm{PH}}^{\mathrm{out,hot}}\right)=\dot{m}_{\mathrm{PH}}^{\mathrm{cold}}c_p^{\mathrm{cold}}\left(T_{\mathrm{PH}}^{\mathrm{out,hot}}-T_{\mathrm{PH}}^{\mathrm{in,hot}}\right) \tag{23}$$

$$\dot{Q}_{\mathrm{IC}}=\dot{m}_{\mathrm{IC}}^{\mathrm{hot}}c_p^{\mathrm{hot}}\left(T_{\mathrm{IC}}^{\mathrm{in,hot}}-T_{\mathrm{IC}}^{\mathrm{out,hot}}\right)=\dot{m}_{\mathrm{IC}}^{\mathrm{cold}}c_p^{\mathrm{cold}}\left(T_{\mathrm{IC}}^{\mathrm{out,cold}}-T_{\mathrm{IC}}^{\mathrm{in,cold}}\right) \tag{24}$$

where the superscript hot, cold, in and out represent the hot fluid, cold fluid, inlet and outlet of heat exchanger, respectively.

(7) Buffer tank

A buffer tank is used for a better flow matching between pre-compressor and liquid piston, and make sure continuous and steady operation of the system in charge stage. Here, assuming that the buffer tank is designed as thermal insulation, and the mass/energy balance equations are:

$$\sum \dot{m}_{\mathrm{BFT}}^{\mathrm{in}}=\sum \dot{m}_{\mathrm{BFT}}^{\mathrm{out}} \tag{25}$$

$$\sum\left(\dot{m}_{\mathrm{BFT}}^{\mathrm{in}}h_{\mathrm{BFT}}^{\mathrm{in}}\right)=\sum\left(\dot{m}_{\mathrm{BFT}}^{\mathrm{out}}h_{\mathrm{BFT}}^{\mathrm{out}}\right) \tag{26}$$

where $\dot{m}_{\mathrm{BFT}}^{\mathrm{in}}$ and $\dot{m}_{\mathrm{BFT}}^{\mathrm{out}}$ are the air mass flow rate moved in and out of buffer tank.

3.2 Kalina cycle

Assuming that there is no energy loss in the mixer's separator and diverter, the energy balance equation of these two components are given as follows:

$$\sum_{i}^{2}\dot{m}_{\mathrm{Mixer}}^{\mathrm{in},i}h_{\mathrm{Mixer}}^{\mathrm{in},i}=\dot{m}_{\mathrm{Mixer}}^{\mathrm{out}}h_{\mathrm{Mixer}}^{\mathrm{out}} \tag{27}$$

$$\dot{m}_{\mathrm{SEP}}^{\mathrm{in}} h_{\mathrm{SEP}}^{\mathrm{in}} = \sum_{i}^{2} \dot{m}_{\mathrm{SEP}}^{i,\mathrm{out}} h_{\mathrm{SEP}}^{i,\mathrm{out}} \tag{28}$$

Applying the law of energy conservation, the heat released by the hot fluid is equal to the heat absorbed by cold fluid in the condenser and the high- and low-temperature heat recuperators.

$$\dot{Q}_{\mathrm{CON3}} = \dot{m}_{\mathrm{CON3}} (h_{\mathrm{CON3}}^{\mathrm{in}} - h_{\mathrm{CON3}}^{\mathrm{out}}) \tag{29}$$

$$\dot{Q}_{\mathrm{HTRG}} = \dot{m}_{\mathrm{HTRG}}^{\mathrm{hot}} (h_{10\mathrm{KC}} - h_{11\mathrm{KC}}) = \dot{m}_{\mathrm{HTRG}}^{\mathrm{cold}} (h_{7\mathrm{KC}} - h_{8\mathrm{KC}}) \tag{30}$$

$$\dot{Q}_{\mathrm{LTRG}} = \dot{m}_{\mathrm{LTRG}}^{\mathrm{hot}} (h_{3\mathrm{KC}} - h_{4\mathrm{KC}}) = \dot{m}_{\mathrm{LTRG}}^{\mathrm{cold}} (h_{6\mathrm{KC}} - h_{7\mathrm{KC}}) \tag{31}$$

For the ammonia turbine, the power output and its isentropic efficiency can be expressed as:

$$\dot{W}_{\mathrm{EXP5}} = \dot{m}_{\mathrm{EXP5}} \left(h_{\mathrm{EXP5}}^{\mathrm{in}} - h_{\mathrm{EXP5}}^{\mathrm{out}} \right) \tag{32}$$

$$\eta_{\mathrm{EXP5}} = \frac{h_{\mathrm{EXP5}}^{\mathrm{in}} - h_{\mathrm{EXP5}}^{\mathrm{out}}}{h_{\mathrm{EXP5}}^{\mathrm{in}} - h_{\mathrm{EXP5,s}}^{\mathrm{in}}} \tag{33}$$

Moreover, the energy balance equation of the evaporator is given by

$$\dot{Q}_{\mathrm{EVP3}} = \dot{m}_{air} \sum_{i=2,5,8} (h_i - h_{i+1}) = \dot{m}_{\mathrm{EVP3}}^{\mathrm{cold}} (h_{9\mathrm{KC}} - h_{8\mathrm{KC}}) \tag{34}$$

where h_i is the enthalpy of air flowing out of the air compressor. In the EVP3, due to using an ammonia–water mixture as the working fluid, the more volatile ammonia tends to vaporize first at a lower temperature, followed by the pure water. Also, the temperature of the remaining two-phase liquid rises as the ammonia concentration decreases [25]. Thus, as shown in Fig. 3, a better heat match between the hot side of the compressed air and the cold side of the ammonia–water mixture is established by employing the variable vaporizing temperature characteristic of the ammonia–water mixture [25].

3.3 Heat pump cycle

It was shown in the literature that R245fa yields satisfactory performance in ORC cycles. Thus, it is used as the refrigerant in the absorption sub-cycle in this work to reduce the cost and improve the safety and reliability of the thermal cycle. Moreover, lithium bromide is used as the working medium in the absorption sub-cycle for efficiently recovering low-temperature exhaust heat in the heat pump cycle. Thus,

$$\dot{m}_{\mathrm{CS}} \cdot X_{\mathrm{CS}} = \dot{m}_{\mathrm{DS}} \cdot X_{\mathrm{DS}} \tag{35}$$

where X_{DS} and X_{CS} denote the concentration of the diluted and concentrated solutions, respectively. $\dot{m}_{\mathrm{DS}}$ and $\dot{m}_{\mathrm{CS}}$ are the respective mass flow rates of the diluted and concentrated solutions.

Moreover, according to the law of energy conservation, the mathematical model of the energy consumed and released in the heat pump cycle are given by:

$$\dot{Q}_{\mathrm{EVP1}}+\dot{Q}_{\mathrm{GEN2}}=\dot{Q}_{\mathrm{ABS}}+\dot{Q}_{\mathrm{CON1}} \tag{36}$$

where $\dot{Q}_{\mathrm{EVP1}}$ and $\dot{Q}_{\mathrm{GEN2}}$ are the energy consumed by the evaporator and generator, respectively. $\dot{Q}_{\mathrm{ABS}}$ and $\dot{Q}_{\mathrm{CON1}}$ represent the respective heat released from the absorber and condenser. The energy conservation laws of these components are as follows:

$$\dot{Q}_{\mathrm{EVP1}}=\dot{m}_{\mathrm{EVP1}}^{\mathrm{hot}}\cdot\left(h_{\mathrm{EVP1}}^{\mathrm{hot,in}}-h_{\mathrm{EVP1}}^{\mathrm{hot,out}}\right)=\dot{m}_{\mathrm{EVP1}}^{\mathrm{cold}}\cdot\left(h_{\mathrm{4HP}}-h_{\mathrm{3HP}}\right) \tag{37}$$

$$\dot{Q}_{\mathrm{EVP2}}=\dot{m}_{\mathrm{EVP2}}^{\mathrm{hot}}\cdot\left(h_{\mathrm{EVP2}}^{\mathrm{hot,in}}-h_{\mathrm{EVP2}}^{\mathrm{hot,out}}\right)=\dot{m}_{\mathrm{EVP2}}^{\mathrm{cold}}\cdot\left(h_{\mathrm{11HP}}-h_{\mathrm{14HP}}\right) \tag{38}$$

$$\dot{Q}_{\mathrm{ABS}}=\dot{m}_{\mathrm{10HP}}\cdot h_{\mathrm{10HP}}+\dot{m}_{\mathrm{vap}}\cdot h_{\mathrm{4HP}}-\dot{m}_{\mathrm{6HP}}\cdot h_{\mathrm{6HP}}=\dot{m}_{\mathrm{air}}\cdot\sum_{i=17,20,23,26}\left(h_{i+1}-h_{i}\right) \tag{39}$$

$$\dot{Q}_{\mathrm{GEN2}}=\dot{m}_{\mathrm{CS}}\cdot h_{\mathrm{9HP}}+\dot{m}_{\mathrm{vap}}\cdot h_{\mathrm{1HP}}-\dot{m}_{\mathrm{DS}}\cdot h_{\mathrm{DS4}}=\dot{m}_{\mathrm{12HP}}\cdot\left(h_{\mathrm{12HP}}-h_{\mathrm{13HP}}\right) \tag{40}$$

$$\dot{Q}_{\mathrm{CON1}}=\dot{m}_{\mathrm{vap}}\cdot\left(h_{\mathrm{1HP}}-h_{\mathrm{2HP}}\right) \tag{41}$$

$$\dot{Q}_{\mathrm{CON2}}=\dot{m}_{\mathrm{CON2}}^{\mathrm{hot}}\cdot\left(h_{\mathrm{12HP}}-h_{\mathrm{13HP}}\right) \tag{42}$$

where h_i and $\dot{m}_{\mathrm{vap}}$ are the inlet enthalpy of air and the steam flow rate, respectively.

3.4 Exergy model of system

Furthermore, the exergy analysis can characterize the exergy destruction in each process of the proposed system, and aids in controlling energy loss during thermal desalination. The method of exergy analysis presented in this study neglects the kinetic and potential exergy. On this basis, the exergy of the material streams in the proposed system can be expressed as follows:

$$\dot{E}x_{ix}=\dot{E}x_{ix}^{\mathrm{ph}}+\dot{E}x_{ix}^{\mathrm{ch}} \tag{43}$$

where the physical exergy $\dot{E}x_{ix}^{\mathrm{ph}}$ and chemical exergy $\dot{E}x_{ix}^{\mathrm{ch}}$ are expressed as:

$$\dot{E}x_{ix}^{\mathrm{ph}}=\dot{m}\left[h_{ix}-h_{0}-T_{0}\left(s_{ix}-s_{0}\right)\right] \tag{44}$$

$$\dot{E}x_{ix}^{\mathrm{ch}}=\dot{m}\left[\sum_{jx}y_{jx}\xi^{0}+RT_{0}\sum_{jx}y_{jx}\ln y_{jx}\right] \tag{45}$$

where y_{jx} and ξ^{0} denote the mole fraction and the standard chemical exergy of the involved chemical component, respectively. For the proposed system, the exergy balance equation is applicable to each component, and is given by:

$$\dot{E}x^{Q}+\sum\dot{m}_{\mathrm{in}}e_{\mathrm{in}}=\dot{E}x^{W}+\sum\dot{m}_{\mathrm{out}}e_{\mathrm{out}}+\dot{E}x^{D} \tag{46}$$

where $\dot{E}x^{Q}$, $\dot{E}x^{W}$, and $\dot{E}x^{D}$ are the input exergy contained in the thermal energy, output net work

and exergy destruction, respectively.

3.5 Performance evaluation criteria

The system's electrical efficiency helps determine the major contributors to energy losses, and thus, it allows the process to be readjusted to improve the overall thermodynamic efficiency. It is defined as the ratio of the total electricity extracted from the system to the total electricity input [4, 26].

$$\eta_{\mathrm{ETE}} = \frac{\sum \dot{W}_{\mathrm{out}}}{\sum \dot{W}_{\mathrm{in}}} \tag{47}$$

Moreover, the exergy efficiency indicates the losses and the internal irreversibilities that should be assessed to improve the system's performance. It is defined as the ratio between all of the exergy products and the total exergy consumption extracted from the proposed system [26].

$$\eta_{\mathrm{EE}} = \frac{\sum \dot{E}x_{p,\mathrm{tot}}}{\sum \dot{E}x_{c,\mathrm{tot}}} \tag{48}$$

4. Results and Discussion

The proposed system uses the Kalina cycle to convert the compressed heat into electricity, in addition to employing the thermal energy storage unit to store thermal energy at a relatively low temperature. The thermodynamic analysis, including the energy analysis and the exergy analysis of the proposed system, is presented and evaluated in this section. In this regard, the simulation conditions of the proposed system are listed in Table 1. According to the computing analysis, the electrical efficiency and exergy efficiency at simulation condition is 63.28% and 59.13%, respectively.

Table 1 The simulation condition of the proposed system.

Term	Unit	Value
Charge stage time	h	8
Discharge stage time	h	4
Isentropic efficiency of compressor	-	0.84
Isentropic efficiency of expander	-	0.88
Isentropic efficiency of EXP5	-	0.87
Isentropic efficiency of COMP4	-	0.75
Efficiency of water pump	-	0.85
Compression ratio	-	2.6
Inlet pressure of BFT	kPa	1600
Initial pressure of AST	kPa	5000
Maximum pressure of AST	kPa	8000
Inner diameter of LP	m	2.2
Height of LP	m	5.8

Inner diameter of BFT	m	2.2
Height of BFT	m	5.8
Volume of AST	m^3	500
Pinch temperature of condensation	K	5
Ambient temperature	K	298.15
Ambient pressure	kPa	101.325
Group number of LP	-	15

4.1 Energy distribution analysis

The energy flow of the proposed system mainly involves two aspects: (i) the energy consumption module, and (ii) the energy generation module. This reflects the energy matching level. Fig. 4 presents an energy flow analysis for the proposed system, breaking down the energy distribution into the relative contributions of each module component. The main energy consumption from the waste heat (WH) used for the heat pump cycle occupies about 40.2% of the overall consumption. This is followed by the power consumption of the pre-compressor, which accounts for 37.6%. In addition, the power consumption for water pumping in the liquid piston accounts for only 20.4% of the total energy consumption. This is a little less than the pre-compressor consumption since the air in the liquid piston is compressed in a near-isothermal process. However, the pre-compressor is operating based on an adiabatic compression mode, and is thus characterized by a relatively low energy efficiency. Moreover, in the power output module, the energy produced by the air expander accounts for 93.6%, of which the waste heat provides the dominant contribution towards power production. In addition, the thermal energy stored in the TES and the energy driven by the HP cycle account for 41.7% and 4.7% of the total power output by the expander, respectively.

As shown in the presented results, the HP cycle and the TES play an important role in operating the proposed compressed air energy storage system at a higher efficiency. In this regard, the electricity consumed for driving the HP cycle has a little effect on the total power output, which accounts for only 4.7%. A KC cycle works by absorbing compressed heat and generating approximately 6.4% of total power output as electricity. Thus, it is necessary to use a waste heat recovery cycle as part of the proposed energy storage system to improve the thermal performance. These research results provide key reference significance for other compressed air energy storage applications.

For a waste-heat source of constant temperature, the thermal energy storage performance

determines the power generation of the system and has a vital effect on the compressed heat allocation between the KC cycle and the TES in the charge stage. Fig. 5 depicts the thermal energy allocation of each sub-cycle in the proposed system under different thermal energy storage temperatures. It is noted that the TES temperature remains below 373.15 K for protection from water evaporation. With the decrease in the TES temperature, a gradual increase is observed in the thermal energy used for driving the KC cycle, waste heat (HP_H), and electricity (HP_E) consumption in the HP cycle. On the other hand, the thermal energy stored in the TES decreases due to the decreasing storage temperature. In this case, the evaporator absorbs more thermal energy to drive the whole KC cycle, leading to a lower storage temperature. On the contrary, these tendencies toward change cause inadequate pre-heating of the high-pressure air in the discharge stage. This in turn leads to an increased demand for reheat energy, and thus more power consumption, including the waste heat necessary for the HP cycle.

On the other hand, a large amount of low-temperature waste heat with difficult recycling makes it difficult to be fully utilized in industrial applications. Thus, a higher heat pump temperature rise (the temperature difference between the waste heat source and the cold stream at the outlet of the condenser, TD-HP) plays an important role in expanding the application of waste heat in industrial production. It is also one of the most important parameters in HP design. Assuming that the temperature of the waste heat source is constant, Fig. 6 shows the thermal energy allocation of each sub-cycle in the proposed system under different TD-HPs. It is noted that the thermal energy and electrical energy consumed for driving the HP cycle decrease significantly with the decrease in the TD-HP. This is because the mass flow rates of both steam and the concentrated solution in the absorber decrease. Furthermore, the thermal energy stored in the TES and consumed to power the KC cycle is kept nearly constant. This indicates that the TD-HP has a little effect on the charging performance. Yet, it is important to take into consideration the impact of the TD-HP on the discharge performance of the proposed system. The results highlight that the thermal energy and the power consumption of the HP cycle decrease by nearly 24.7% and 20.9%, respectively, as the TD-HP decreases from 45 K to 35 K. This reflects the energy consumption in the HP cycle change with an equivalent magnitude.

4.2 Thermodynamic performance of liquid piston

In the charging stage, the liquid piston has an important role in further enhancing the air pressure.

In addition, the variations of the pressure, mass flow rate, and temperature of the air inside the liquid piston have a direct influence on the whole charging process (Figs. 7 to 10). As shown in Table 1, a charging stage of the proposed system lasts 8 hours, and the thermal parameters vary dramatically in this stage. Specifically, in the compression and expansion stages, the pressure in the liquid piston changes significantly. On the contrary, the pressure in the buffer tank (BFT) exhibits a nearly sawtooth oscillation at a low amplitude. This demonstrates that the near-isothermal compression dominates the charging process in the proposed system and is conditioned by the pre-set value of pressure. On this basis, the superior thermal performance of the proposed system is primarily devoted to the isothermal compression process. In addition, the pressure and temperature of air in the liquid piston vary in a sawtooth oscillation pattern, and seem to grow in the air storage tank (AST) by some degrees until the charging is over. The total mass of air inside the BFT always remains higher than that in the liquid piston. Moreover, in the energy holding and discharging phases, the thermal conditions of the working medium in the liquid piston are kept almost unchanged. On the other hand, the air inside the AST decreases significantly in the discharge stage.

Nevertheless, the air temperature variation in the liquid piston is an important indicator for its thermal state evaluation. As shown in Fig. 8, the air temperature in the liquid piston increases above 30 K in the compression stage. On the other hand, the temperature rises in the adiabatic compression process and reaches 250 K while the air is compressed from 1.5 MPa to 8 MPa. Compared to the case with the liquid piston, the temperature of the air inside the AST is characterized by smaller variations due to the full exchanger. In this regard, the maximum temperature difference in the AST is less than 5 K. This validates the constant temperature assumptions for AST in most studies in the literature. In the discharge stage, the air temperature inside the AST decreases and stays below the ambient air temperature. As shown in Fig. 10, the air inside the AST has twice the flow of that of the single liquid piston. This indicates that the liquid piston can simultaneously achieve the technical requirements of high efficiency and a large flux using one pump.

4.3 Thermal performance analysis

Overall, ammonia-water has different thermophysical properties under different operational conditions. Thus, as the circulating working medium of the KC cycle, the inlet pressure of the ammonia turbine has a great influence on the evaporation temperature, evaporation pressure, and the overall system performance in the cycle. Fig. 11(a) shows the effect of the ammonia turbine inlet

pressure on the system's performance. It is noted that the electrical efficiency and exergy efficiency of the system increase gradually with the increase in the inlet pressure of the ammonia turbine. The reason for this thermal performance variation is devoted to the increased power generation in the KC cycle, as shown in Fig. 11(a).

In the proposed system, an adiabatic compressor and a liquid piston are assembled to compress air. Thus, the performance in the charging stage is primarily affected by the air pressure entering and leaving the liquid piston. In addition, the power consumption of the water pump and the compressor at 7 MPa and 8 MPa outlet pressures of the liquid piston is depicted in Fig. 11(b). In this case, the power consumption of the water pump and the compressor increases with the increase in the inlet pressure of the liquid piston. It should be noted that a higher outlet pressure results in a higher power consumption in the water pump. Furthermore, the amount of electricity consumed in the adiabatic compression process is significantly greater than the amount consumed in the water pumping process, especially when the liquid piston has a high outlet pressure. However, in the charging stage, the air is compressed primarily in the liquid piston, which illustrates that the near-isothermal compression process plays a key role in the proposed system. In addition, compared with the compressor, the power consumed by the water pump shows a slight increase with the increase in the inlet pressure. This indicates that the potential energy in the compressed air energy storage system is not a major energy storage carrier.

Furthermore, Fig. 12 shows the effect of the ammonia-water concentration and the water storage temperature on the system performance. It is shown that the increase in the ammonia-water concentration leads to an increase in the electrical efficiency and exergy efficiency of the system due to the increase in the mass flow rate in the KC cycle. Although the increase in the ammonia-water concentration is beneficial to the system's thermal performance, it is demonstrated that it is not useful to have a higher ammonia mass concentration. When the mass concentration of ammonia is close to 1, the thermodynamic properties of ammonia-water are to some extent close to the properties of pure ammonia, and its corresponding phase change temperature slip value decreases, At the same time, it will gradually lose the advantage of variable temperature phase change with a larger heat transfer loss between the working medium and the cold heat source. These conditions lead to the heat exchange performance of the heat source in the generator being close to the performance of pure ammonia.

This means that the heat exchange area of the generator and the system's investment costs increase significantly. In addition, the storage temperature of the TES has a direct effect on the energy distribution of each sub-system. Combined with the results shown in Fig. 5, it is shown that the increase in the storage temperature of the TES leads to a significant reduction in the energy consumption for driving the HP cycle. This is the main factor causing the increase in the system operation efficiency characterized by Eq. (47). It is also noted that for a storage temperature of 357 K, the electrical efficiency shows a slower increase compared to the case with a temperature of 349 K. On the other hand, the ammonia-water concentration increases from 0.8 to 0.9. As highlighted in Section 4.1, the heat generated in the compression process is first used to drive the KC cycle, and the remaining thermal energy is stored in the TES. On this basis, most of the compression heat is absorbed by the KC cycle for a lower storage temperature mode. Thus, the variation in the ammonia-water concentration has a significant impact on the system's performance.

Noticeably, for the proposed system, the operation efficiency of Kalina cycle is only 16%; this means that electric generation from Kalina cycle only accounts for merely 5% of total energy consumption in charge stage. As shown in Fig. 12, the ammonia concentration impact on the system performance is relatively small, as the efficiency is changed on the hundredths of the digit. This illustrates that the ammonia concentration of Kalina cycle is not the dominant factor for improving the system performance.

In the conducted analysis, it was assumed that the inlet temperature of the compressor, the wall temperature of the liquid piston, and the temperature of the cooling water are constant at a certain ambient air temperature. As the ambient air temperature increases, the electrical efficiency and the exergy efficiency decrease correspondingly (Fig. 13). This is because the thermal performance of air compression in the liquid piston deteriorates, and both the electricity consumed for driving pumps and the compression heat produced in the process are severely wasted. As shown in Fig. 13, the increase in the temperature of the waste source leads to a changing trend of the exergy efficiency. The exergy efficiency first increases and then decreases. Thus, there exists an optimal value for the waste heat source temperature at which the proposed system operates at its optimal conditions. This is because the coefficient of performance of the HP cycle increases with the increase in the waste heat source temperature, as reflected in the rising trend. However, the heat transfer rate and the heat transfer temperature difference in the absorber increase continuously following the growth

of the waste heat source temperature. As a result of these phenomena, the amount of energy destroyed increases. In contrast to the exergy efficiency variation trend, the system's electrical efficiency increases linearly with increasing waste source temperature. Therefore, a positive correlation can be deduced between the outlet temperature of the regenerator and the waste source temperature in the proposed system. This results in increased power generation from the air turbine.

Under different heat source temperature scenarios, the thermal storage temperature leads to a clearly different effect on the electrical efficiency and the exergy efficiency, as shown in Fig. 14. When the heat source temperature is 359 K and the storage temperature in the TES changes from 349 K to 359 K, the electrical efficiency extreme point occurs at a temperature of 353 K. In addition, increasing the storage temperature is shown to cause the power consumption in the KC cycle to decrease faster than in the HP cycle (shown in Fig. 5), thus increasing the electrical efficiency. However, as the storage temperature continues to increase, the power consumption of the driving HP cycle also increases rapidly. This eventually leads to a decrease in the electrical efficiency. It is also noted that the electrical efficiency increases monotonically by setting the heat source temperature lower.

Furthermore, the exergy efficiency of the system increases linearly with the increase in the storage temperature of the TES. However, it is noted that at a storage temperature of 355 K, the same exergy efficiency is achieved for both the 339 K and 359 K heat seat source temperatures. In addition, when the storage temperature exceeds 355 K, the exergy efficiency at a 339 K heat source temperature is found to be larger than that at 339 K, but lower with a lower storage temperature.

Nevertheless, the ability to raise the temperature (ΔT) of the heated medium in the HP cycle is an important indicator for the cycle evaluation and has a significant effect on the performance of the whole proposed system, as shown in Fig. 15. As ΔT increases, the electrical efficiency is found to increase monotonically. However, the exergy efficiency of the proposed system follows the opposite trend. In this regard, the exergy efficiency decreases slowly first and then exhibits a sharp decline with the increase in ΔT . This is because the initial increase in the temperature difference ΔT causes the decrease in the coefficient of performance of the HP, and thus a slight decrease in the exergy efficiency. However, as ΔT increases further, the exergy destruction in the regenerator and the HP cycle decreases significantly. This decreasing trend becomes even more striking at a higher heat source temperature. It is worth noting that an excessive high-temperature difference

ΔT will lead to a higher circulation rate in the HP cycle, which is not conducive to actual circulation.

Fig. 16 presents the effect of the inlet pressure of the liquid piston on the system performance. As the inlet pressure increases, the electrical efficiency and the exergy efficiency both increase monotonically. The trend of efficiency increase slows down due to the decreasing compression ratio of the liquid piston. Noticeably, for a constant liquid piston inlet pressure, a larger storage pressure in the AST leads to a better thermal performance. However, this trend weakens as the storage pressure increases. The reason for this is related to the energy consumption of the water pump and the pre-compressor, as depicted in Fig. 11.

5. Conclusions

ACAES systems are considered to provide an effective energy storage means for delivering several hours of power at a plant-level output scale. In this study, a modified ACAES system with a near-isothermal pressurized boosting air and a KC cycle reusing compression heat in the charging process was proposed to further improve energy utilization. A dynamic performance model of the proposed system was developed to detail the transient behavior of each component. The calculation results showed that the waste heat used to drive the HP cycle has the largest share in terms of energy consumption among all the system components. Moreover, the adiabatic compressor is the key component for achieving energy storage, yet near-isothermal compression in the liquid piston realizes exergy storage primarily. In addition, a KC cycle with a 6.4% electricity generation and a TES using water as the thermal storage medium are used for cascade utilization of compression heat. This will largely improve the performance of the system. It was demonstrated that a TES storage temperature of 353 K and a heat source temperature of 345 K provide the highest electrical efficiency and exergy efficiency. Increasing the concentration of ammonia-water to a certain extent is an effective way to further improve energy utilization.

Nevertheless, the proposed system and the obtained results provide a reference for the optimal energy allocation in the charging and discharging processes of CAES. These research results are useful for guiding the development of the proposed technology and will be useful for further exploring the off design performance, and improving the configuration and components' integration of the proposed system in the future. Noticeably, in this proposed system, the heat pump subsection comprises a R245fa cycle, however this gas has a high GWP and is gradually superseded by HFO

or natural fluids. Besides, the thermo-economic performance and multiple-objective optimization of the proposed system should be further considered, which not only can find out the problem that energy be exhausted, but also can direct the energy conversion. Besides,

Nomenclature

A	Area
D	Internal diameter
F	Shape factor
Gr	Grashof number
h	Enthalpy
H	Height
k	Isentropic Exponent
$\dot{m}$	Mass flow rate
Nu	Nusselt number
p	Pressure
Pr	Prandtl number
Ra	Rayleigh number
Re	Reynolds number
T	Temperature
U	Heat transfer coefficient
V	Volume
$\dot{W}$	Power

Greek letters

α	Thermal expansion coefficient
η	Efficient
λ	Thermal conductivity
π	Compression/Expansion ratio
μ	Dynamic viscosity
ρ	Density

Subscripts

a	Air
o	Outer
w	Water
amb	Ambient
ave	Average value
CS	Concentrated solution
vap	Vapor

References:

[1] N. Courtois, M. Najafiyazdi, R. Lotfalian, R. Boudreault, and M. Picard, "Analytical expression for the evaluation of multi-stage adiabatic-compressed air energy storage (A-CAES) systems cycle efficiency," *Applied Energy,* vol. 288, 2021.

[2] T. Letcher, and D. Reay, "Storing Energy (Second Edition)," 2022.

[3] T. Neu and A. Subrenat, "Experimental investigation of internal air flow during slow piston compression into isothermal compressed air energy storage," *The Journal of Energy Storage,* vol. 38, p. 102532, 2021.

[4] V. C. Patil and P. I. Ro, "Modeling of liquid-piston based design for isothermal ocean compressed air energy storage system," *The Journal of Energy Storage,* vol. 31, p. 101449, 2020.

[5] J. Wieberdink, P. Y. Li, T. W. Simon, and D. V. Van, James D, "Effects of porous media insert on the efficiency and power density of a high pressure (210bar) liquid piston air compressor/expander – An experimental study," *Applied Energy,* vol. 212, p. 1025-1037, 2018.

[6] P. Li, E. Loth, Q. Chao, T. Simon, and J. Ven, *Open Accumulator Isothermal Compressed Air Energy Storage (OA-ICAES) System*. Wiley Energy Storage Handbook, 2018.

[7] V. C. Patil, J. Liu, and P. I. Ro, "Efficiency improvement of liquid piston compressor using metal wire mesh for near-isothermal compressed air energy storage application," *The Journal of Energy Storage,* vol. 28, p. 101226, 2020.

[8] G. Venkataramani, P. Vijayamithran, Y. Li, Y. Ding, H. Chen, and V. Ramalingam, "Thermodynamic analysis on compressed air energy storage augmenting power / polygeneration for roundtrip efficiency enhancement," *Energy,* vol. 180, p. 107-120, 2019.

[9] J. Sun, H. Hou, Z. Zuo, H. Tang, and H. Chen, "Numerical study on wet compression in a supercritical air centrifugal compressor," *Proceedings of the Institution of Mechanical Engineers, Part A: Journal of Power and Energy,* vol. 234, p. 384-397, 2020.

[10] J. A. Bennett *et al.*, "Techno-economic analysis of offshore isothermal compressed air energy storage in saline aquifers co-located with wind power," *Applied Energy,* vol. 303, p. 117587, 2021.

[11] G. Dib, P. Haberschill, R. Rullière, and R. Revellin, "Thermodynamic investigation of quasi-isothermal air compression/expansion for energy storage," *Energy Conversion and Management,* vol. 235, 2021.

[12] H. Chen, H. Wang, R. Li, H. Sun, G. Ge, and L. Ling, "Experimental and analytical investigation of near-isothermal pumped hydro-compressed air energy storage system," *Energy,* vol. 249, p. 123607, 2022.

[13] B. Mmha *et al.*, "Analysis and optimization of a modified Kalina cycle system for low-grade heat utilization," *Energy Conversion and Management: X,* vol. 12, 2021.

[14] R. Li, H. Wang, and Q. Tu, "Thermo-Economic Analysis and Optimization of Adiabatic Compressed Air Energy Storage (A-CAES) System Coupled with a Kalina Cycle," *Energy Technology,* 2018.

[15] M. J. Dehghani, "Enhancing energo-exergo-economic performance of Kalina cycle for low- to high-grade waste heat recovery: Design and optimization through deep learning methods," *Applied Thermal Engineering,* vol. 195, p. 117221, 2021.

[16] M. An, X. Zhao, Z. Xu, R. Wang, "A Hybrid Compression-Absorption High Temperature Heat Pump Cycles for Industrial Waste Heat Recovery," *Journal of Shanghai Jiao Tong University,* vol. 55, p. 434~443, 2021.

[17] A. Odukomaiya, A. Abu-Heiba, S. Graham, and A. M. Momen, "Experimental and analytical evaluation of a hydro-pneumatic compressed-air Ground-Level Integrated Diverse Energy Storage (GLIDES) system," *Applied Energy,* vol. 221, p. 75-85, 2018.

[18] A. Odukomaiya, "Comprehensive Simulation and Experimental Characterization of Various Configurations of a Ground-Level Integrated Diverse Energy Storage (GLIDES) System," 2018.

[19] A. Lefevre, J. P. B. Mota, A. J. S. Rodrigo, and E. Saatdjian, "Chaotic advection and heat transfer enhancement in Stokes flows," *International Journal of Heat & Fluid Flow,* vol. 24, p. 310-321, 2003.

[20] A. Vallati, R. Vollaro, P. Oclon, and J. Taler, "Experimental and Analytical Evaluation of a Gas-Liquid Energy Storage (GLES) Prototype," *Energy,* p. 120061, 2021.

[21] A. Odukomaiya, E. Kokou, Z. Hussein, A. G. Abu-Heiba, S. D. Graham, and A. M. Momen, "Near-isothermal-isobaric compressed gas energy storage," *The Journal of Energy Storage,* vol. 12, p. 276-287, 2017.

[22] S. W. Churchill and M. Bernstein, "A Correlating Equation for Forced Convection From Gases and Liquids to a Circular Cylinder in Crossflow," *Asme Transactions Journal of Heat Transfer,* vol. 99, p. 300-306, 1977.

[23] R. Winterton, "Where did the Dittus and Boelter equation come from?," *International Journal of Heat & Mass Transfer,* vol. 41, p. 809-810, 1998.

[24] J. R. Lloyd and W. R. Moran, "Natural Convection Adjacent to Horizontal Surface of Various Planforms," *Journal of Heat Transfer,* vol. 96, p. 443, 1974.

[25] P. Zhao, J. Wang, and Y. Dai, "Thermodynamic analysis of an integrated energy system based on compressed air energy storage (CAES) system and Kalina cycle," *Energy conversion & management,* vol. 98, p. 161-172, 2015.

[26] R. Li, H. Wang, and H. Zhang, "Dynamic simulation of a cooling, heating and power system based on adiabatic compressed air energy storage," *Renewable Energy,* vol. 138, p. 326-339, 2019.

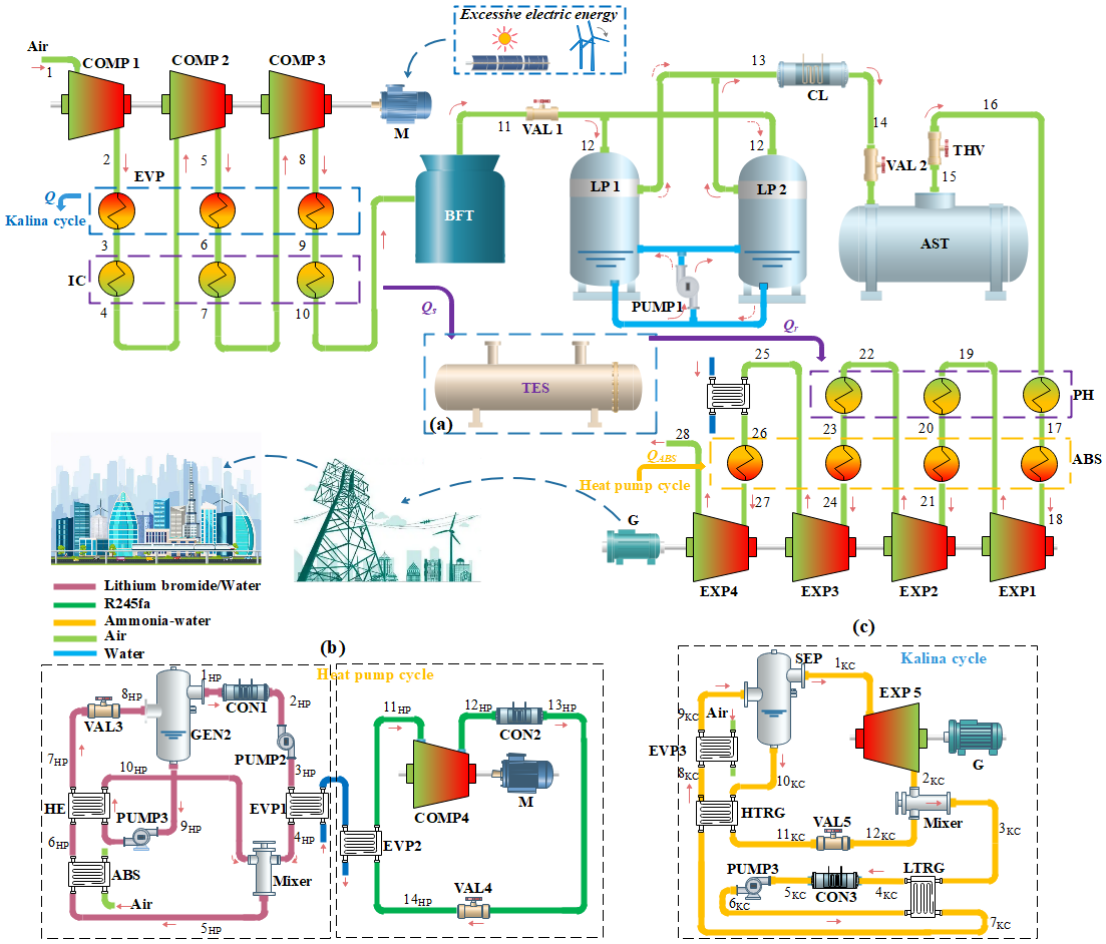

COMP-Compressor; IC-Intercooler; BFT-Buffer tank; LP-Liquid piston; AST-Air storage tank; VAL-Valve; THV-Throttle valve; EXP-Expander; PH-Preheater; GEN-Steam generator; ABS-Absorber; EVA-Evaporator; CL-Cooler; PUMP-Pump; SEP-Separator; CON-Condenser; M-Motor; G-Generator; HTRG-high-temperature regenerator; LTRG-low-temperature regenerator; HE- Heat exchanger.

Fig. 1 Schematic of proposed energy system. (a) Thermal energy storage subsystem; (b) Heat pump cycle subsystem; (c) Kalina cycle subsystem.

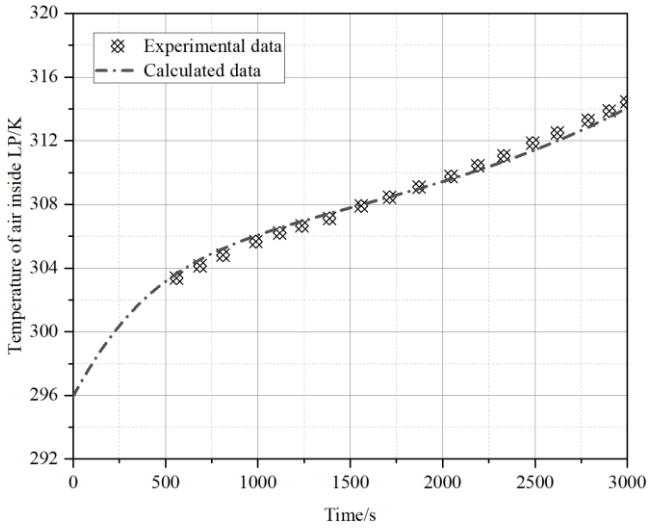

Fig. 2 Comparing the experimental results with the calculation analysis.

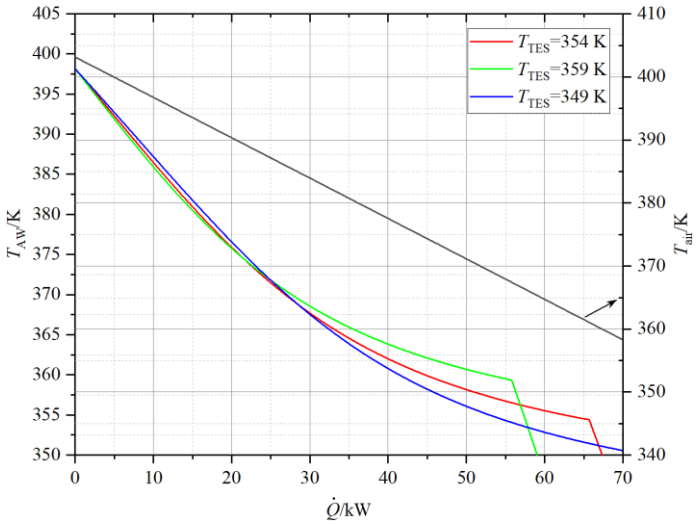

Fig. 3 Compressed air/ammonia–water temperature profile.

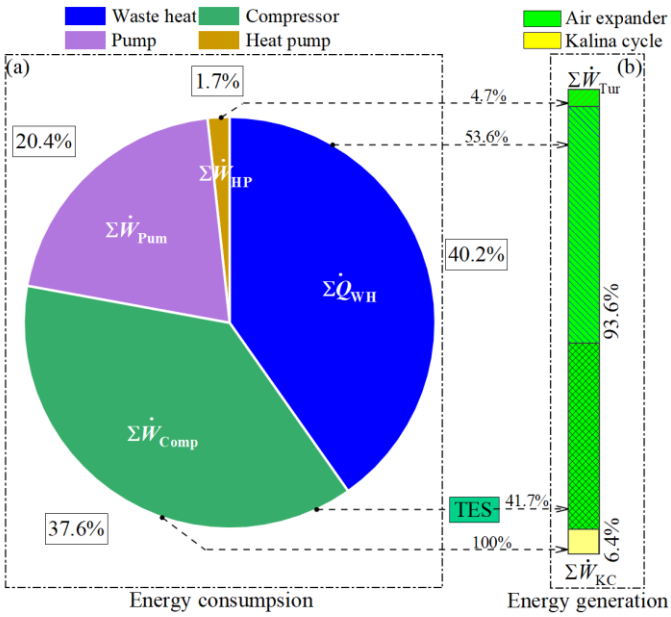

Fig. 4 Energy distribution of the proposed system. (a) stands for the energy consumption components in the proposed system; (b) is the energy generation components; the lines that go from energy consumption modular to energy generation modular mean energy contributions.

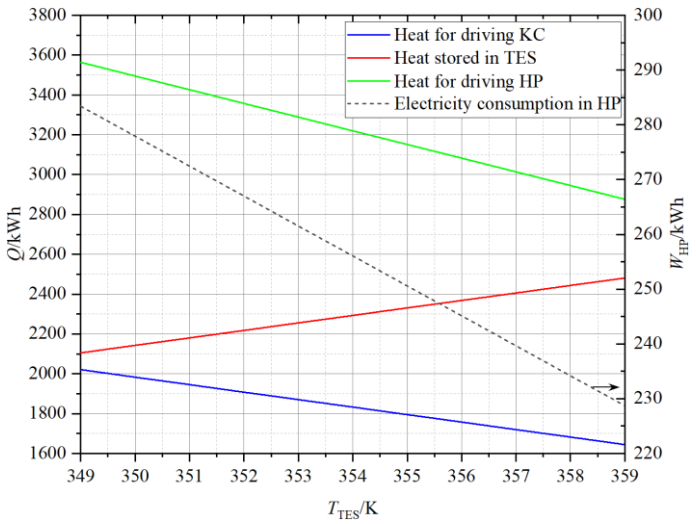

Fig. 5 Energy consumption of each subsystem under different thermal energy storage temperature.

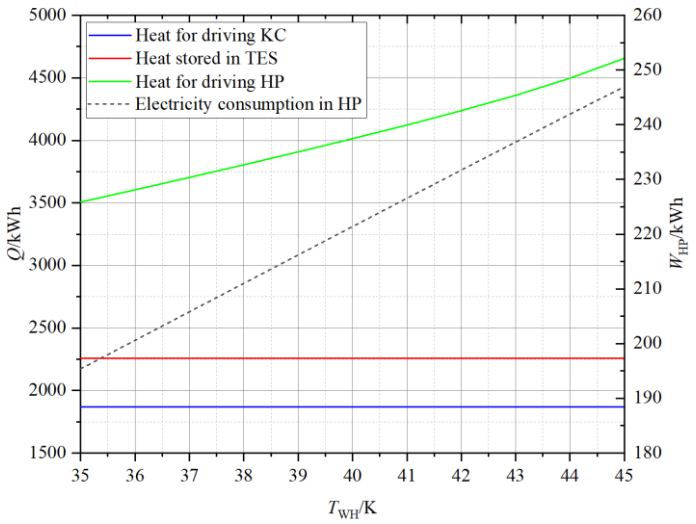

Fig. 6 Energy consumption of each subsystem under different heat source temperature.

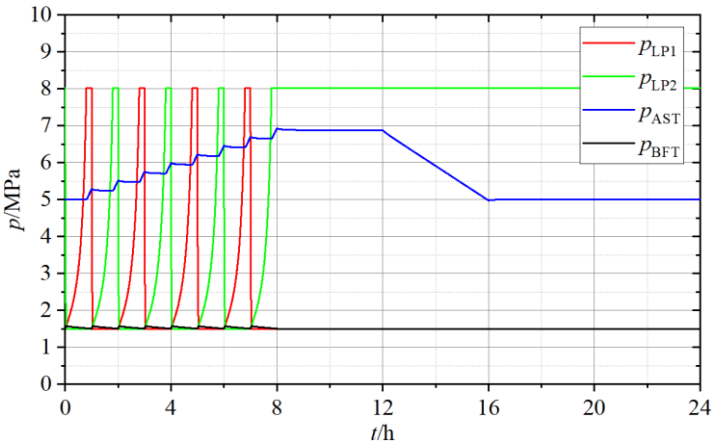

Fig. 7 Pressure variation of LP1, LP2, BFT and AST in charge stage.

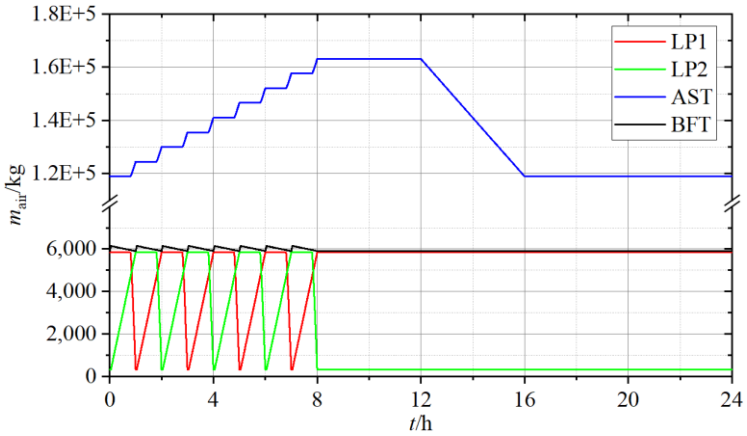

Fig. 8 Mass variation of air inside LP1, LP2, BFT and AST in charge stage.

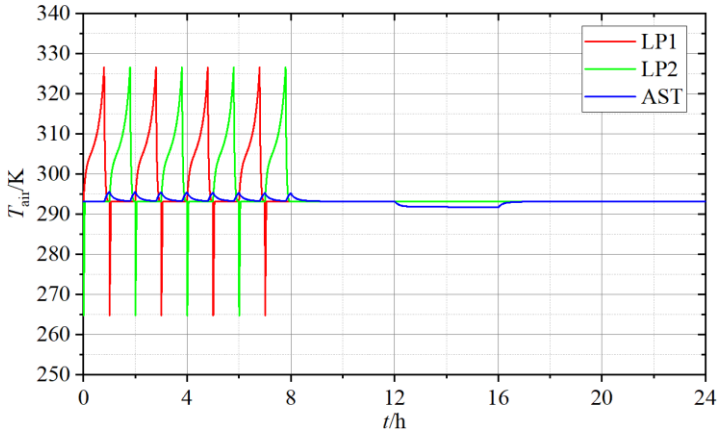

Fig. 9 Temperature variation of air inside LP1, LP2 and AST in charge stage.

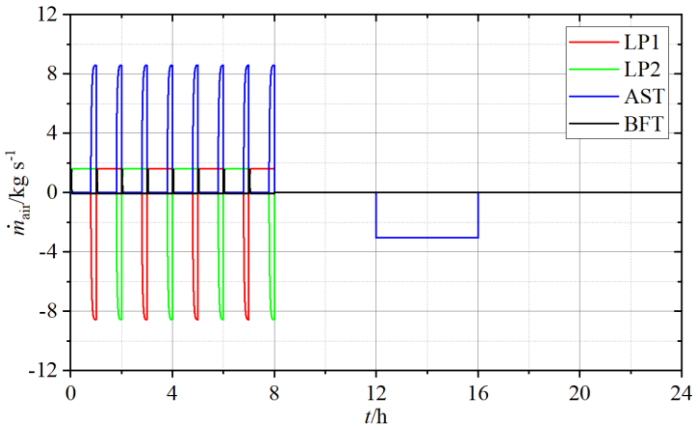

Fig. 10 Mass flow rate variation of air inside LP1, LP2, BFT and AST in charge stage.

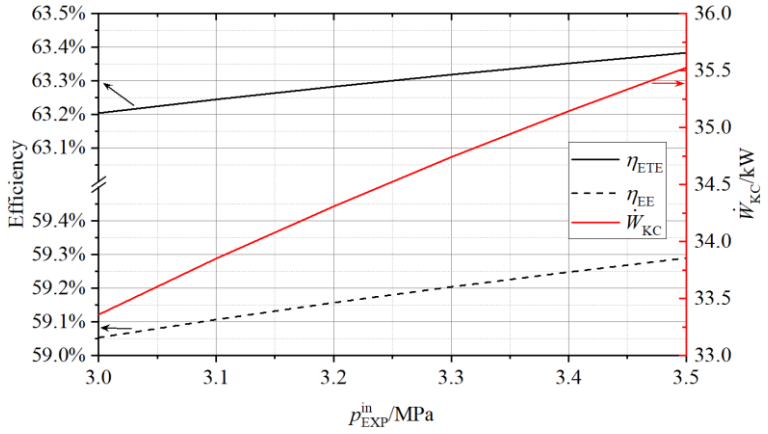

(a)

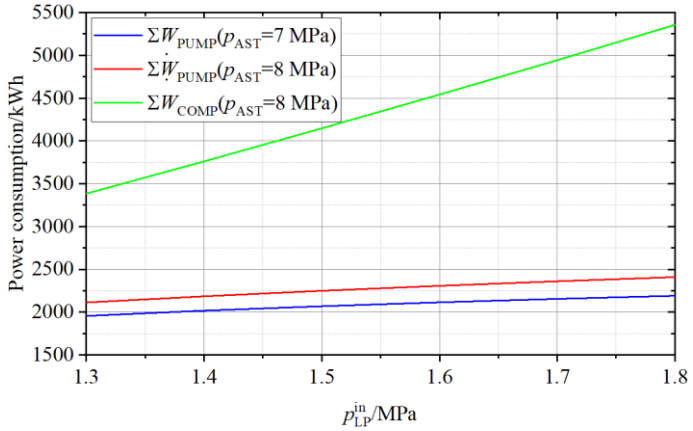

(b)

Fig. 11 Effect of the inlet pressure of ammonia turbine and liquid piston. (a) Effect of the inlet pressure of ammonia turbine on the system performance; (b) Effect of the inlet pressure of liquid piston on the energy consumption of water pump and pre-compressor.

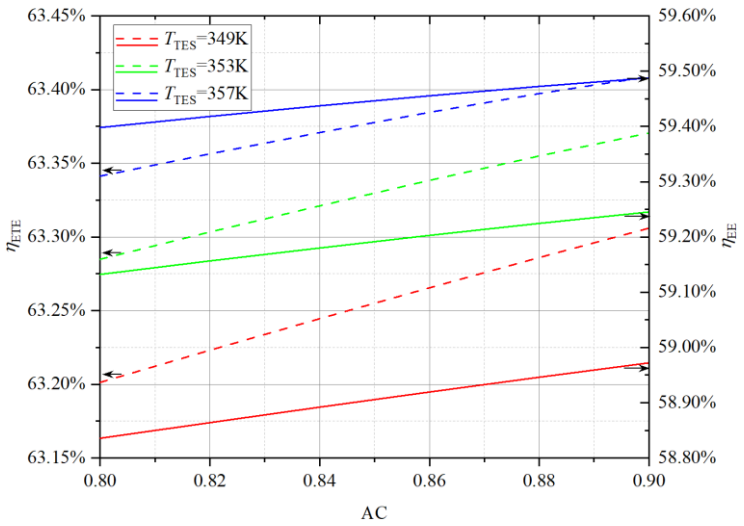

Fig. 12 Effect of ammonia concentration on the system performance.

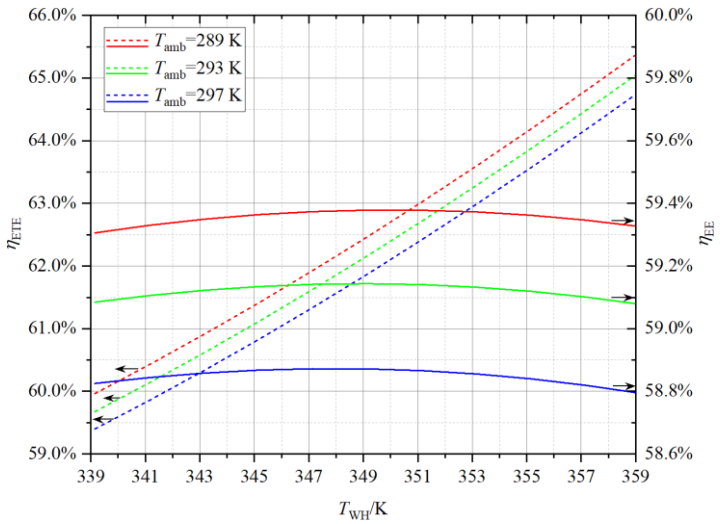

Fig. 13 Effect of heat source temperature on system performance.

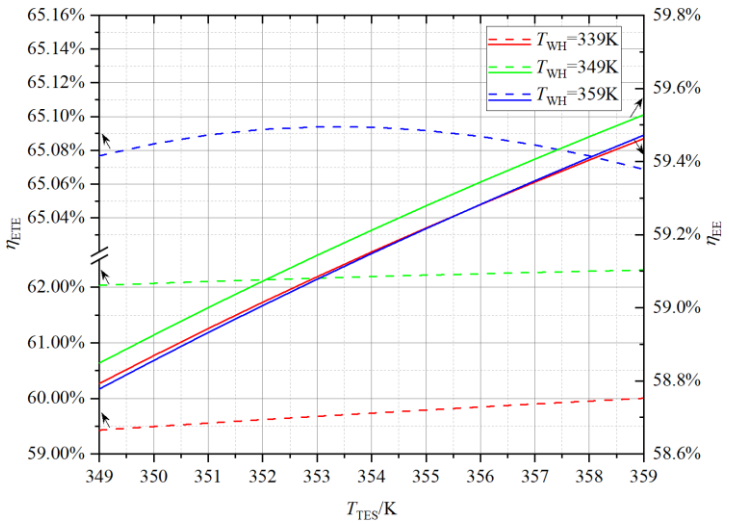

Fig. 14 Effect of thermal energy storage temperature on system performance.

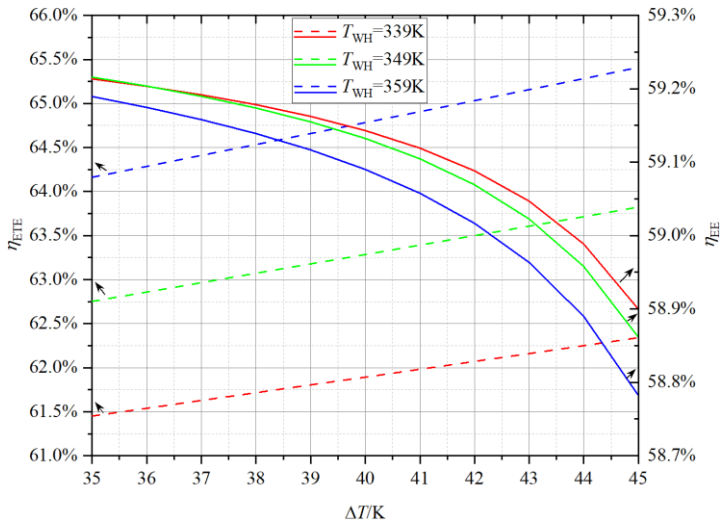

Fig. 15 Effect of temperature difference of cold fluid in ABS on system performance.

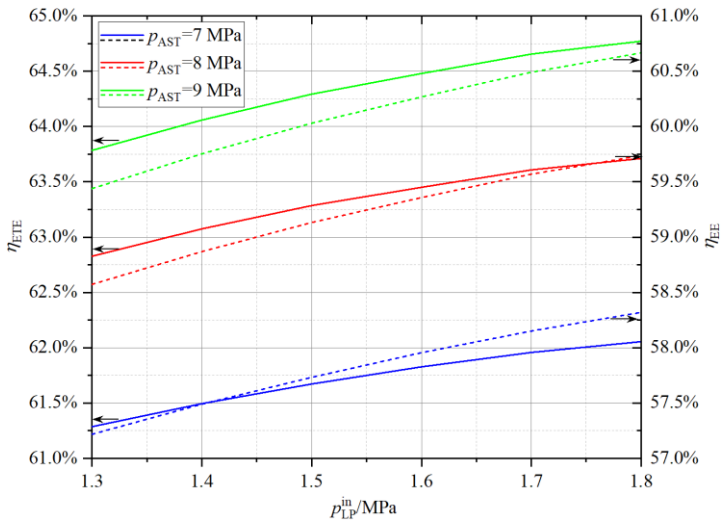

Fig. 16 Effect of the inlet pressure of liquid piston on system performance.